PIER C

(Received 23 November 2025, Accepted 4 February 2026, Scheduled 6 April 2026)

Dual-Band Meander Antenna for IoT and 5G Sub-6 GHz Applications

Abdellah Elabdi[1], Abdenasser Lamkaddem[2], Moussa El Ayachi[1], Mohammed Rahmoun[1], Mohammed Ali Ennasar[3], Otman El Mrabet[3], Anuar M. Kassim[4, 5, *], and A. J. A. Al-Gburi[6, *]

[1] *Applied Science Research Laboratory, National School of Applied Sciences, Mohamed I University, Oujda, Morocco*
[2] *Signal Theory and Communication Department, University Carlos III of Madrid, 28911 Madrid, Spain*
[3] *Information and Telecommunication Systems Lab, Faculty of Sciences, Abdelmalek Essaadi University, Tetouan, Morocco*
[4] *Center of Robotics and Industrial Automation, Faculty of Technology and Electrical Engineering Universiti Teknikal Malaysia Melaka, Hang Tuah Jaya, 76100 Durian Tunggal, Melaka, Malaysia*
[5] *IngeniousCity Engineering Solutions (ICES), Sdn. Bhd. No 79-1, Jalan Satu Krubong Taman Satu Krubong, 75250 Krubong, Melaka, Malaysia*
[6] *Strategic Research Institute (SRI), Asia Pacific University Jalan Teknologi 5, Taman Teknologi Malaysia, 57000 Kuala Lumpur, Malaysia*

ABSTRACT: The efficient integration of wireless communication technologies into IoT applications is essential to ensuring seamless and reliable access to application data. In this context, the present paper proposes a dual-band meander-shaped patch antenna, specifically designed for IoT applications. The proposed antenna supports operation across the WLAN, 4G, and 5G frequency bands, with resonant frequencies centered around 2.4 GHz and 5 GHz. The design is implemented on a Rogers RT-5880 substrate, and all simulations and optimizations are performed using CST Microwave Studio (CST MWS). The antenna features compact dimensions of $20 \times 10 \times 1.57\,\text{mm}^3$ (equivalent to $0.16 \times 0.08 \times 0.01\lambda_0^3$ at 2.4 GHz). The proposed antenna's effectiveness was assessed through a comprehensive evaluation combining numerical simulations and experimental prototyping. Its performance outcomes were further benchmarked against contemporary designs reported in recent literature. Distinguished by its miniaturized geometry, straightforward integration into electronic platforms, cost-effectiveness, and manufacturability, the antenna demonstrates strong potential for deployment in advanced Internet of Things (IoT) infrastructures.

1. INTRODUCTION

Compact devices equipped with miniature antennas have become essential for Internet of Things (IoT) applications, due to their compatibility with a wide range of cases [1–4]. Among the challenges encountered, particular attention is given to applications operating at low frequencies, where the inverse relationship between antenna size and operating frequency poses significant constraints [5, 6]. In this context, antenna miniaturization emerges as a key solution to meet these requirements. Several techniques have been developed to reduce antenna size, including the use of meandered lines [3, 4, 7, 8], fractal structures [9, 10], and metamaterials [11, 12]. The miniaturization technique used in this study is based on the implementation of meandered lines. Antennas designed using this approach allow for significant size reduction, both of the antenna itself and the devices in which they are integrated, while maintaining acceptable radiation performance. In applications where compactness and size reduction are critical requirements, meandered-line antennas are particularly advantageous, as they effectively extend the electrical path of the radiating element within a confined physical area. These antennas are well-suited for a wide range of wireless applications, including mobile devices, short-range wireless communication networks, and IoT devices [7–9]. The reviewed academic works span a comprehensive range of investigations into compact antenna architectures and optimization strategies applicable to wireless communication and IoT platforms. In [13], a miniaturized linearly polarized antenna for ultra-high frequency radio frequency identification (UHF RFID) mobile phones is proposed, with dimensions of $75 \times 16 \times 10\,\text{mm}^3$ ($0.23 \times 0.05 \times 0.03\lambda^3$). A multiband microstrip antenna, incorporating defected ground structures (DGS) and patch slots, is proposed in [14]; it measures $55.5 \times 42.75 \times 1.5\,\text{mm}^3$ ($0.44 \times 0.34 \times 0.01\lambda^3$). In [15], the authors describe a miniaturized internal monopole antenna measuring $40 \times 10 \times 0.8\,\text{mm}^3$ ($0.44 \times 0.11 \times 0.02\lambda^3$), offering a multi-resonant response suitable for Internet of Things (IoT) applications and providing a wide bandwidth for various wireless communication scenarios. Article [16] introduces a compact antenna for radio frequency (RF) energy harvesting, with dimensions of $37 \times 20 \times 1.6\,\text{mm}^3$ ($0.29 \times 0.16 \times 0.01\lambda^3$). Furthermore, a compact meandered antenna optimized for 2.45 GHz resonance is presented in [17]; it measures $35 \times 35 \times 1.6\,\text{mm}^3$ ($0.28 \times 0.28 \times 0.01\lambda^3$) and delivers wide bandwidth and exhibits elevated radiation efficiency, rendering it well-suited for wireless sensor networks and RFID systems. Finally, article [18] introduces an ultra-narrowband filter/antenna hybrid designed for long-range radio (LoRa) applications in the ultra-high frequency (UHF) band. This component stands out for its exceptional compactness and high frequency selectivity, with dimensions of $25 \times 40 \times 1.524\,\text{mm}^3$ ($0.07 \times 0.12 \times 0.004\lambda^3$).

* Corresponding authors: Ahmed Jamal Abdullah Al-Gburi (ahmedjamal@ieee.org); Anuar Mohamed Kassim (anuar@utem.edu.my).

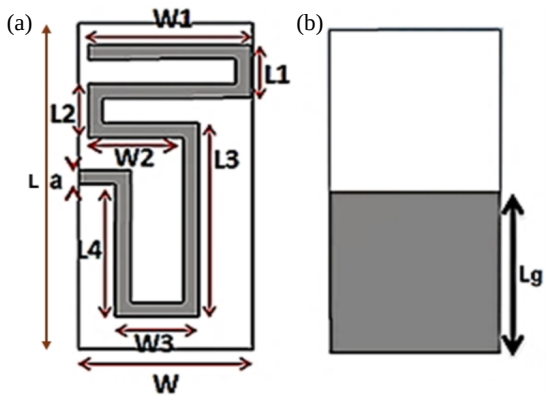

FIGURE 1. Geometry of the proposed antenna: (a) top view; (b) ground plane.

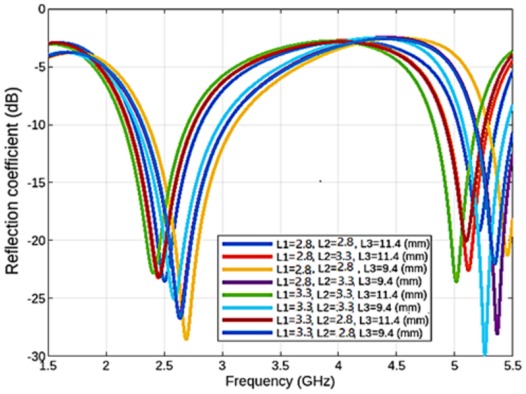

FIGURE 2. The frequency-dependent performance of the proposed antenna with respect to parameters $L1$, $L2$, and $L3$.

Collectively, these studies highlight the diversity of approaches available for designing efficient, compact, and adaptable antennas to address the growing requirements of wireless communication and IoT technologies. In this work, we present a $20 \times 10 \times 1.57\,\text{mm}^3$ ($0.16\lambda \times 0.08\lambda \times 0.01\lambda$) patch antenna with a ground plane of $10 \times 10\,\text{mm}^2$ ($0.08\lambda \times 0.08\lambda$), making it particularly suitable for dynamic wireless networks supporting IoT and 5G applications. This work is a continuation of our earlier work [3], adding manufacturing and expanding the frequency domain while verifying the findings through measurements. The antenna construction is composed of a meander-shaped structure constructed on a low-cost double-sided Rogers RT5880 substrate (thickness of 1.57 mm, loss tangent of 0.0009, and relative permittivity of 2.2). The WLAN 4G and 5G frequency bands (2.4 GHz and 5.1 GHz) are where it operates. Because of its compact design and affordable price, the suggested solution is a great fit for the growing need for IoT-focused dynamic wireless network systems. The simulation is performed using Microwave Studio simulators from Computer Simulation Technology (CST). The results obtained are confirmed by realization and measurement.

2. ANTENNA DESIGN

2.1. Structural Configuration of the Proposed Antenna

This antenna is designed on a Rogers RT5880 substrate of 1.57 mm thickness, featuring a relative permittivity of 2.2 and a very low loss tangent of 0.0009. CST high-frequency modeling software was used for its design and simulation. Table 1 lists the optimized dimensions. The physical layout of the proposed antenna is shown in Figure 1, where the ground plane is limited to half of the substrate area ($10 \times 10\,\text{mm}^2$), and a meandering-line radiator is placed on the other side. The antenna is excited using a microstrip feeding line.

TABLE 1. Optimized antenna parameters.

Symbol	L	Lg	$L1$	$L2$	$L3$	$L4$
Value (mm)	20	10	3.3	3.3	11.9	8.1
Symbol	W	$W1$	$W2$	$W3$	a	h
Value (mm)	10	9.5	5.5	4.8	0.9	1.57

2.2. Effect of the Dimensions *L1*, *L2* and *L3*

The graph in Figure 2 illustrates the effect of lengths $L1$, $L2$, and $L3$ on the resonant frequency of an antenna with widths $W1$, $W2$, $W3$, and Lg fixed at 9.5 mm, 5.5 mm, 6.8 mm, and 10 mm, respectively. Target frequencies are set at 2.4 GHz and 5.1 GHz. Each curve in the graph represents a different configuration of these lengths, noted in millimeters. The reflection coefficient $|S_{11}|$ is plotted as a function of the frequency, reflecting the degree of impedance matching of the antenna to the desired frequency band. From the graph, it is clear that varying the lengths of $L1$, $L2$, and $L3$ has a significant impact on the resonant frequency. The minimum values of $|S_{11}|$, which represent the points of the best impedance matching, shift as a function of these lengths. Adjustments are required to bring the resonance precisely to 2.4 GHz and 5.1 GHz. For configurations where $L1$, $L2$, and $L3$ have small values, 2.8 mm, 2.8 mm, and 9.4 mm, respectively, we have a maximum resonance frequency compared with the other combinations. For configurations where $L1$, $L2$, and $L3$ have large values, 3.3 mm, 3.3 mm, and 11.4 mm, respectively, we have a minimum resonance frequency compared with the other combinations. This implies that decreasing the lengths $L1$, $L2$, and $L3$ increases the resonance, and vice versa. To ensure operation at the desired frequency, the dimensions of $L1$, $L2$, and $L3$ are assigned values of 3.3 mm, 3.3 mm, and 11.4 mm respectively.

2.3. Influence of Widths *W1*, *W2* and *W3*

Figure 3 illustrates the effect of the widths $W1$, $W2$, and $W3$ on the antenna's resonant frequency, with target frequencies set at 2.4 GHz and 5.1 GHz. During the analysis, the lengths $L1$, $L2$, $L3$, and Lg were fixed at 3.3 mm, 3.3 mm, 9.4 mm, and 10 mm, respectively. Optimizing the widths $W1$, $W2$, and $W3$ is essential for accurately achieving the desired resonant frequencies. Based on the simulation results, the optimal values for these widths were determined to be 9.5 mm for $W1$, 5.5 mm for $W2$, and 4.8 mm for $W3$.

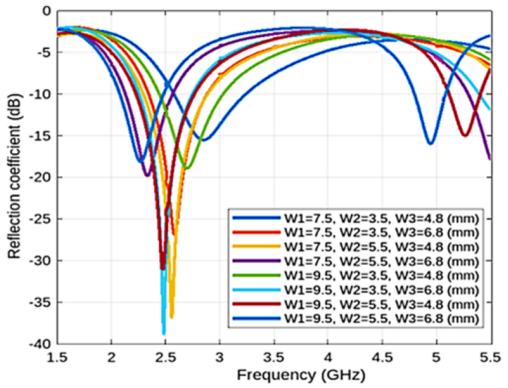

FIGURE 3. A parametric study of $W1$, $W2$, and $W3$ on the performance of the proposed antenna across frequency.

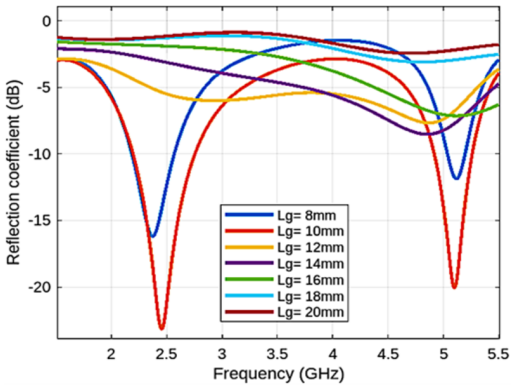

FIGURE 4. Impact of Lg on the antenna behavior as a function of frequency.

(a)

(b)

FIGURE 5. Images of the fabricated antenna prototype: (a) top view and (b) bottom view.

2.4. Influence of the *Lg* Parameter

The graph in Figure 4 illustrates the effect of ground plane length (Lg) on the resonant frequency and reflection coefficient $|S_{11}|$ of an antenna, with parameter values $W1$, $W2$, $W3$, $L1$, $L2$, and $L3$ fixed at 9.5 mm, 5.5 mm, 6.8 mm, 3.3 mm, 3.3 mm, and 9.4 mm, respectively. Each curve represents a different length of the ground plane, indicated in millimeters. As can be seen, varying Lg strongly affects the antenna's resonance characteristics. For example, when Lg is set to 10 mm (orange curve), the antenna reaches the smallest $|S_{11}|$ value at around 2.4 GHz, indicating the best impedance matching and minimum reflection at this frequency. Conversely, shorter or longer ground plane lengths, such as 8 mm (blue curve) or 20 mm (red curve), shift the resonant frequency and degrade matching performance. This analysis shows that optimizing the ground plane length is crucial to achieving the desired resonant frequency with optimum antenna performance.

3. RESULTS AND DISCUSSIONS

The parametric analysis of the key design variables is presented as follows: the effects of the resonator lengths $L1$, $L2$, and $L3$ are shown in Figure 2; the effects of the strip widths $W1$, $W2$, and $W3$ are detailed in Figure 3; and the effect of the ground plane length Lg is presented in Figure 4. As seen in Figure 2, it is demonstrated that the resonant frequencies of the suggested antenna are determined by lengths $L1$, $L2$, and $L3$. Lengths $L1$, $L2$, and $L3$ are assigned values of 3.3 mm, 3.3 mm, and 11.4 mm, respectively, to ensure the target frequency. Figure 3 illustrates how the widths $W1$, $W2$, and $W3$ affect the frequency bands in a similar manner. $W1$, $W2$, and $W3$ have widths of 9.5 mm, 5.5 mm, and 4.8 mm, in that order. Additionally, Figure 4 shows how frequency values and antenna matching are affected by ground plane length Lg. 10 mm is chosen as the final length of Lg.

3.1. Realization and Validation of Results

This section presents the fabricated prototype of the proposed antenna. The antenna was realized on a Rogers RT-5880 substrate, characterized by a loss tangent of 0.0009, a thickness of 1.57 mm, and a relative permittivity of 2.2. Using a standard chemical etching process, the fabrication involved the use of Ferric chloride ($FeCl_3$) as the primary etching agent to remove unwanted copper from the substrate surface, forming the desired antenna structure. This process ensures good surface quality and accurate dimensional control of the antenna structure. The prototype is shown in Figure 5. The reflection coefficient $|S_{11}|$ of the proposed antenna was characterized using a Vector Network Analyzer (VNA) to evaluate its impedance matching and operating bandwidth, as illustrated in Figure 6. For

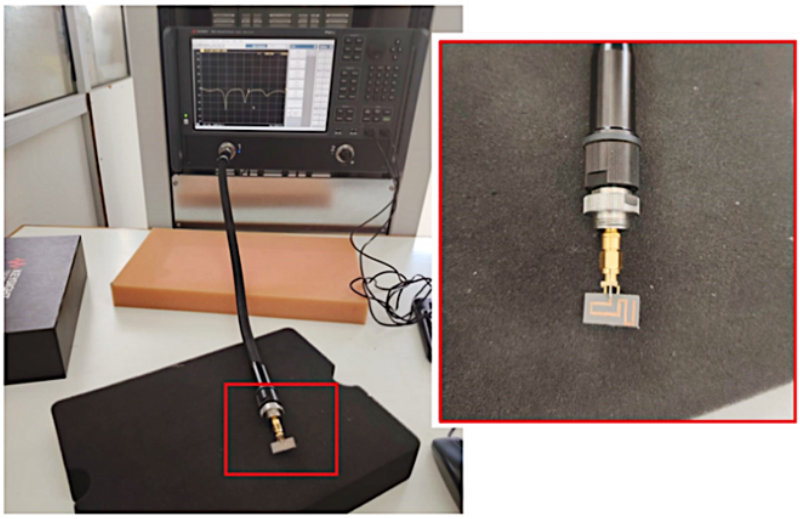

FIGURE 6. $|S_{11}|$ measurement setup for the proposed antenna.

radiation pattern measurements, a standard horn antenna was used as the transmitting antenna, while the proposed antenna served as the receiving antenna. The VNA is from Keysight. We calibrated the VNA using the electronic calibration. The horn antenna has a gain of 18 dBi around the functioning frequency band. The distance between the transmitter (Tx) and Data Transmission Unit (DTU) is 2 m to ensure clean far-field conditions.

Figure 7 presents the total efficiency of the antenna on a linear scale. The antenna achieves the peak efficiency of approximately 14% around 3 GHz, while maintaining efficiencies of about 10–13% at the target operating bands of 2.4 GHz and 5 GHz. The reduced efficiency at lower and higher frequencies is mainly attributed to impedance mismatch and increased losses outside the resonant bands.

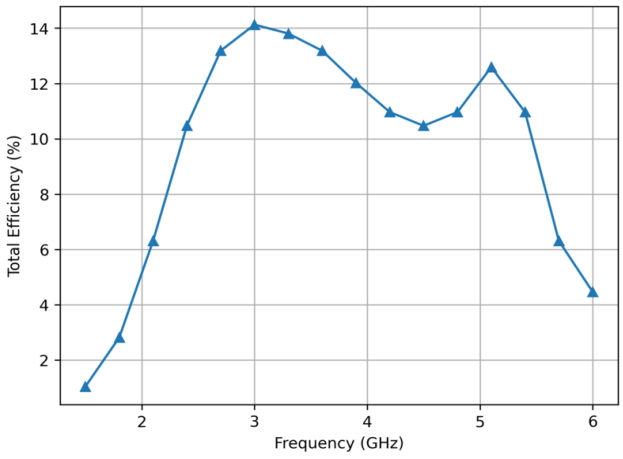

FIGURE 7. Total efficiency of the proposed antenna.

Free-space radiation pattern measurements of the fabricated antenna were performed using the setup depicted in Figure 8. The device under test (DUT) was rotated in the azimuth plane while being illuminated by a fixed-position horn antenna, enabling the acquisition of both E-plane and H-plane patterns. The excellent concordance between the measured results and simulated models serves to validate the design.

Figure 9 shows the $|S_{11}|$ performance of the proposed antenna, showing a comparison between simulation and measurement data. The simulated curve (solid blue line) demonstrates two operating bands around 2.4 GHz and 5 GHz, while the measured curve (orange dashed line) follows a similar trend with slight frequency shifts, particularly near 5 GHz. These deviations can be attributed to fabrication tolerances and environmental factors. The small discrepancies, especially around 5 GHz, are likely due to limitations of the chemical etching process, which may introduce minor dimensional inaccuracies during the fabrication of compact antenna structures.

Radiation diagrams show a generally good match between measurements and simulations, although discrepancies remain, mainly in the shape of the lobes. These differences may indicate efficiency losses, interference, or variations in experimental conditions compared with theoretical models.

Table 2 compares the proposed antenna with several compact antennas specifically designed for Internet of Things (IoT) applications. Refs. [13–17] have larger overall dimensions than our antenna, while [13, 15, 17, 18] exhibit narrower bandwidths. These factors demonstrate that our antenna offers a significant advantage compared to the referenced works. As presented in Table 3, variations in the geometrical parameters

TABLE 2. Estimated resonant frequencies for each parameter ($L1$, $L2$, $L3$).

$L1$ (mm)	$L2$ (mm)	$L3$ (mm)	Res. 1 (GHz)	Res. 2 (GHz)
2.8	2.8	11.4	2.65	5.2
2.8	2.8	9.4	2.75	5.3
2.8	3.3	9.4	2.6	5.1
3.3	3.3	11.4	2.55	5.0
3.3	3.3	9.4	2.7	5.2
3.3	2.8	11.4	2.6	5.1
3.3	2.8	9.4	2.8	5.4

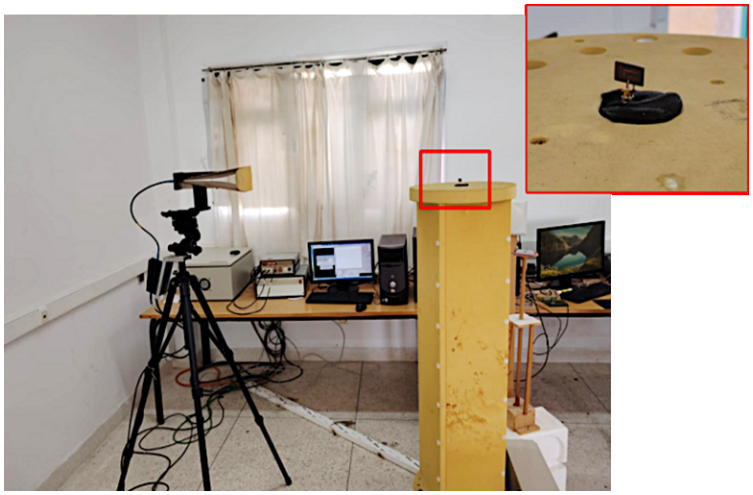

FIGURE 8. Measured radiation pattern of the proposed antenna.

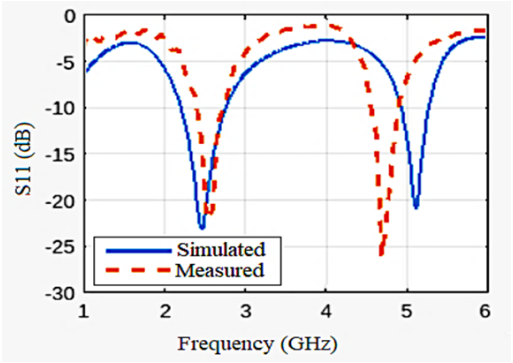

FIGURE 9. Comparison of measured and simulated reflection coefficients ($|S_{11}|$).

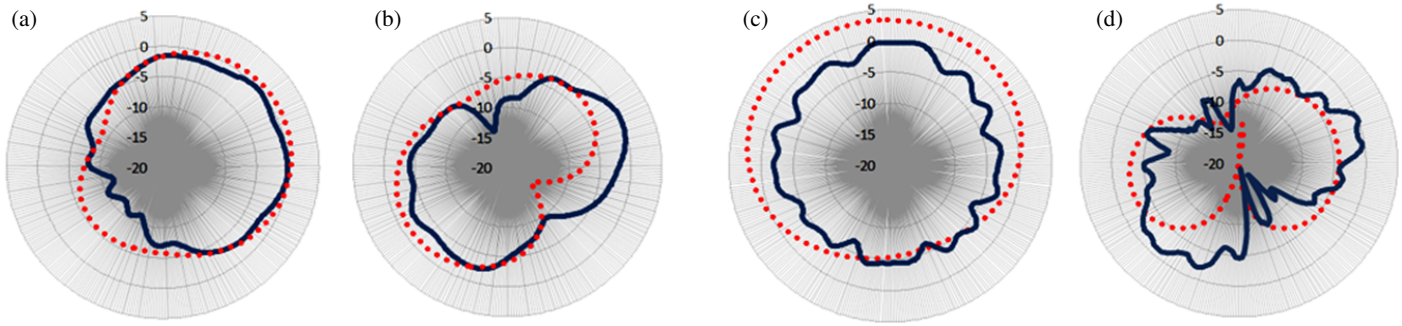

FIGURE 10. Radiation pattern with measured directivity (in dBi) in 2D of the proposed antenna, compared with the simulation at 2.4 GHz: (a) in the E plane, (b) in the H plane, and 5.1 GHz: (c) in the E plane, (d) in the H plane.

TABLE 3. Estimated resonant frequencies for each parameter ($W1$, $W2$, $W3$) .

$W1$ (mm)	$W2$ (mm)	$W3$ (mm)	Res. 1 (GHz)	Res. 2 (GHz)
7.5	3.5	4.8	2.8	5.8
7.5	3.5	6.8	2.7	5.6
7.5	5.5	4.8	2.65	5.55
7.5	5.5	6.8	2.5	5.5
9.5	3.5	4.8	2.7	5.8
9.5	3.5	6.8	2.5	5.8
9.5	5.5	6.8	2.4	5.0

$W1$, $W2$, and $W3$ significantly affect the estimated resonant frequencies, demonstrating clear tuning behavior for both the first and second resonance modes.

4. ANTENNA TESTING IN A REALISTIC ENVIRONMENT

For IoT applications, the antenna has been tested in a realistic environment, where it is connected to the NRF24L01 transceiver device linked to an Arduino Uno. Figure 10 shows

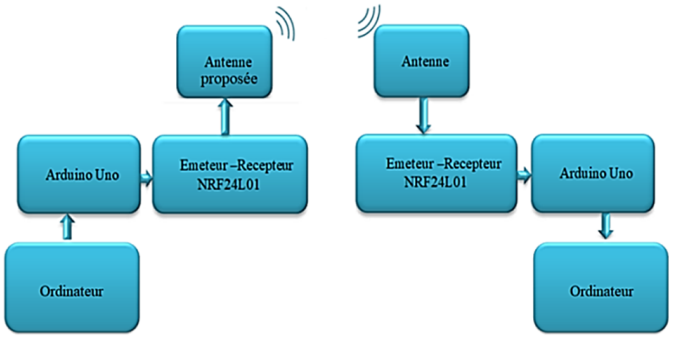

FIGURE 11. Block diagram for communication between Arduino Uno devices using the proposed antenna, where the resonance frequency is 2.4 GHz.

the communication block diagram between two Arduino Uno devices using the proposed antenna as a transmitter antenna, illustrated in Figure 11, designed for IoT applications. The system is made up of several interconnected components that work together to transmit and receive data efficiently. Figure 12 presents the experimental setup and successful data transmission between two Arduino Uno devices using the fabricated antenna at 2.4 GHz.

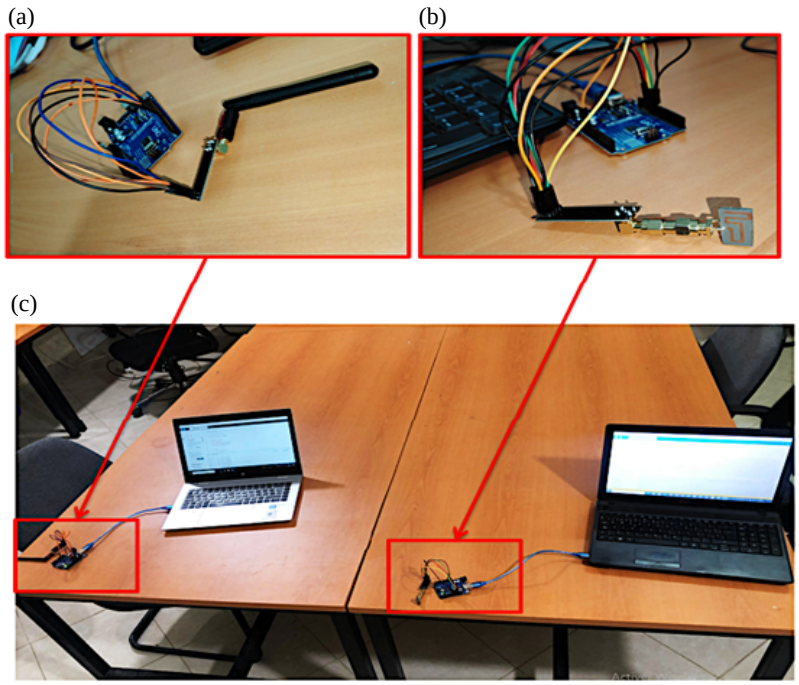

FIGURE 12. (a) Receiving antenna, (b) transmitting antenna, and (c) data communication from the Arduino Uno device using the fabricated meandre antenna with a resonant frequency of 2.4 GHz.

TABLE 4. A comparison of the proposed antenna's performance and the available literature.

Ref.	Year	Size (λ_0^3)	Substrate Material	Frequency (GHz)	BW (%)	$\lvert S_{11}\rvert$
[13]	2020	$0.23 \times 0.05 \times 0.03$	F4B	0.915	2.84	-39
[14]	2021	$0.44 \times 0.34 \times 0.01$	Rogers RO3003	2.44 5.19 5.9	N.A	-33.9 -39.5 -24.7
[15]	2021	$0.44 \times 0.11 \times 0.02$	FR-4	3.3 4.6	15.38 10.98	-18 -14
[16]	2021	$0.29 \times 0.16 \times 0.01$	N.A	2.45	133	-19
[17]	2023	$0.28 \times 0.28 \times 0.01$	FR-4	2.45	8.09	-31.67
[18]	2024	$0.07 \times 0.12 \times 0.004$	Rogers 4003	0.868	4.2	-16
This work	2025	$0.08 \times 0.16 \times 0.01$	Rogers RT-5880	2.5 4.7	12.8 7.4	-22.1 -26.1

On one side, a computer is connected to an Arduino Uno transmits data. The Arduino Uno processes this data and transmits it to the NRF24L01 transceiver module. This wireless module takes the data processed by the Arduino Uno and sends it via our proposed antenna in the case of a resonant frequency of 2.4 GHz. The associated control block adjusts the antenna parameters to guarantee the 2.4 GHz bandwidth, as the NRF24L01 only operates on this frequency. Our fabricated antenna plays a crucial role in transmitting RF signals containing message data sent by the computer. These signals are then received by an antenna on the other side of the communication. The NRF24L01 module, associated with this receiving antenna, picks up the signals and transmits the received data to a second Arduino Uno. Once the data has been received by the Arduino Uno on the receiving side, it is processed and displayed by the computer as a received message. The wireless transmission test at 2.4 GHz clearly demonstrates the effectiveness of the proposed antenna. It provides stable and reliable communication between NRF24L01 modules, with good reception quality and precise bandwidth management. These results confirm that this compact antenna is well-suited for IoT applications, ensuring optimal performance in real-world environments. As shown in Table 4, the proposed antenna exhibits competitive performance in terms of size, bandwidth, and impedance matching compared with existing literature. The use of a Rogers RT-5880 substrate enables efficient dual-band operation while maintaining a compact electrical size.

5. CONCLUSION

The design of a dual-band, meander-shaped patch antenna appropriate for Internet of Things applications was the goal of this study. This antenna, which is based on a Rogers RT-5880 substrate, covers the WLAN, 4G, and 5G spectrum and functions effectively in the 2.4 GHz and 5 GHz frequency bands. With its overall dimensions of $20\times10\times1.57\,\text{mm}^3$ ($0.16\times0.08\times0.01\lambda_0^3$) at 2.4 GHz, the antenna is notable for its small size, low cost, ease of fabrication, and ease of circuit integration. Manufacturing and measurements verified the simulation results, confirming the expected performance and proving this design's viability for the intended uses.

ACKNOWLEDGEMENT

The authors express their sincere gratitude to Universiti Teknikal Malaysia Melaka (UTeM) and the Ministry of Higher Education (MOHE) of Malaysia for their valuable support in funding and facilitating this project. The authors also extend their appreciation to Asia Pacific University of Technology and Innovation (APU), Malaysia for supporting in enhancing and the development of this research.

REFERENCES

[1] Saeed, N., A. Bader, T. Y. Al-Naffouri, and M.-S. Alouini, "When wireless communication responds to COVID-19: Combating the pandemic and saving the economy," *Frontiers in Communications and Networks*, Vol. 1, 566853, 2020.

[2] Al-Gburi, A. J. A., Z. Zakaria, M. Palandoken, I. M. Ibrahim, A. A. Althuwayb, S. Ahmad, and S. S. Al-Bawri, "Super compact UWB monopole antenna for small IoT devices," *Computers, Materials & Continua*, Vol. 73, No. 3, 2785–2799, 2022.

[3] Nurhayati, N., A. N. D. N. Fahmi, P. Puspitaningayu, O. Wiriawan, B. Raafi'u, F. A. Iskandarianto, A. J. A. Al-Gburi, A. K. Varshney, and S. Johari, "Wearable wideband textile coplanar Vivaldi antenna for medical and IOT application," *Progress In Electromagnetics Research C*, Vol. 148, 145–156, 2024.

[4] Elabdi, A., M. Elayachi, and M. Rahmoun, "Frequency reconfigurable miniature antenna for IoT and 5G applications," in *International Conference on Smart Medical, IoT & Artificial Intelligence*, Vol. 11, 167–175, Springer, Cham, 2024.

[5] Al-Sehemi, A., A. Al-Ghamdi, N. Dishovsky, N. Atanasov, and G. Atanasova, "A flexible miniature antenna for body-worn devices: Design and transmission performance," *Micromachines*, Vol. 14, No. 3, 514, 2023.

[6] Dakhli, S., J. M. Floc'h, M. Aseeri, A. Mersani, and H. Rmili, "Design of compact and superdirective metamaterial-inspired two-and three-elements antenna arrays," *Journal of Electromagnetic Engineering and Science*, Vol. 23, No. 4, 362–368, 2023.

[7] Monisha, R. and B. Bhuvaneshwari, "Design of meander line antenna for wearable applications," in *2018 3rd International Conference on Communication and Electronics Systems (ICCES)*, 623–625, Coimbatore, India, 2018.

[8] Lamkaddem, A., A. E. Yousfi, V. González-Posadas, and D. Segovia-Vargas, "Miniaturized dual band implantable antenna for implanted biomedical devices," *IEEE Access*, Vol. 12, 15 026–15 036, 2024.

[9] Khade, S. S., S. Tembhare, P. Gawali, S. Jain, R. Ingole, and C. V. Bawankar, "Dual band meander line antenna for 5G and WLAN application," in *2023 International Conference on Computer, Electronics & Electrical Engineering & their Applications (IC2E3)*, 1–5, Srinagar Garhwal, India, 2023.

[10] Malek, N. A., N. A. C. Sabri, M. R. Islam, S. Y. Mohamad, and F. N. M. Isa, "Design of hybrid koch-minkowski fractal dipole antenna for dual band wireless applications," in *2019 IEEE Asia-Pacific Conference on Applied Electromagnetics (APACE)*, 1–5, Melacca, Malaysia, 2019.

[11] Liu, K., D. Sun, T. Su, X. Zheng, and C. Li, "Design of flexible multi-band miniature antenna based on minkowski fractal structure and folding technique for miniature wireless transmission system," *Electronics*, Vol. 12, No. 14, 3059, 2023.

[12] Ripin, N., W. M. A. W. Saidy, A. A. Sulaiman, N. E. A. Rashid, and M. F. Hussin, "Miniaturization of microstrip patch antenna through metamaterial approach," in *2013 IEEE Student Conference on Research and Developement*, 365–369, Putrajaya, Malaysia, 2013.

[13] Yan, Y., A. Sharif, J. Ouyang, C. Zhang, and X. Ma, "UHF RFID handset antenna design with slant polarization for IoT and future 5G enabled smart cities applications using CM analysis," *IEEE Access*, Vol. 8, 22 792–22 801, 2020.

[14] Refaat, S. M., A. Abdalaziz, and E. K. I. Hamad, "Tri-band slot-loaded microstrip antenna for internet of things applications," *Advanced Electromagnetics*, Vol. 10, No. 1, 21–28, 2021.

[15] Chung, M.-A. and C.-W. Yang, "A miniaturized planar monopole antenna based on a coupling structure for compact mobile internet of things (IoT) and electric vehicles (EVs) device applications in 5G, LTE, WLAN, WiMAX, Sirius/XM Radio, V2X, and DSRC wireless systems," *International Journal of Antennas and Propagation*, Vol. 2021, No. 1, 7535382, 2021.

[16] Awais, Q., A. Farooq, W. Ali, R. Afzal, and A. Khalid, "A novel wideband coplanar waveguide (CPW) fed antenna for energy harvesting at 2.45 GHz," *Engineering Proceedings*, Vol. 12, No. 1, 54, 2021.

[17] Raina, R., L. K. Baghel, and S. Kumar, "Design and analyses of planar antenna for bluetooth based IoT applications," in *2023 First International Conference on Microwave, Antenna and Communication (MAC)*, 1–5, Prayagraj, India, 2023.

[18] Allabouche, K., F. Fabien, J.-M. Ribero, J. Mohammed, E. A. E. I. Najiba, and L. Lizzi, "Compact high-Q slot loaded dielectric resonator filtering antenna for LoRa applications," *AEU — International Journal of Electronics and Communications*, Vol. 175, 155078, 2024.